Supporting Information

Morphological Self-Assembly of Enantiopure Allenes for Up-standing Chiral Architectures at Interfaces

Yi-Qi Zhang,[a] Murat Anil Öner,[a] Inmaculada R. Lahoz,[b] Borja Cirera,[a] Carlos-Andres Palma,*[a] Silvia Castro-Fernández,[b] Sandra Míguez-Lago,[b] M. Magdalena Cid,[b] Johannes V. Barth,[a] José Lorenzo Alonso-Gómez,*[b] Florian Klappenberger*[a]

[a] *Physik Department E20, Technische Universität München, James-Franck-Straße, 85748 Garching, Germany. E-mail: fklapp@ph.tum.de; c.a.palma@tum.de*

[b] *Departamento de Quimica Orgánica, Universidade de Vigo, 36310 Vigo, Spain. E-mail: lorenzo@uvigo.es.*

Index

General procedures

Solvents were dried according to published methods and distilled before use.[1] All other reagents were commercial compounds of the highest purity available. All reactions were carried out under argon atmosphere, and those not involving aqueous reagents were carried out in oven-dried glassware for at least 12 hours to 140 ºC. All solvents and anhydrous solutions were transferred through syringes and cannula previously dried in the oven for at least 12 h and kept in a desiccator with KOH.

Flash column chromatography (FC) was carried out using Merck Kieselgel 60 (230-400 mesh) under pressure. Analytical thin layer chromatography (TLC) was performed on aluminium plates with Merck Kieselgel $60F_{254}$ and visualized by UV irradiation (254 nm) or by staining with a solution of phosphomolibdic acid. UV/Vis and ECD spectra were recorded on a Jasco J-815 spectropolarimeter at 25 ºC. ^{1}H NMR spectra were recorded at ambient temperature on a Bruker AMX-400 spectrometer at 400 MHz with residual solvent as the internal reference; chemical shifts (δ) are given in parts per million (ppm), and coupling constants (J) are given in Hertz (Hz). The proton spectra are reported as follows: δ (multiplicity, coupling constant J, number of protons, assignment). ^{13}C NMR spectra were recorded at ambient temperature on the same spectrometer at 100 MHz. IR spectra were recorded on a JASCO *FT/IR-4200* infrared spectrometer from a thin film deposited onto a NaCl glass plate Peaks are quoted in wave numbers (cm^{-1}). Mass spectra were performed at CACTI (Universidade de Vigo) by a Hewlett-Packard HP59970 instrument operating at 70 eV by electron ionization and on an APEX III FT-ICR MS (Bruker Daltonics, Billerica, MA) equipped with a 7T actively shielded magnet. Ions were generated using an Apollo API electrospray ionization (ESI) source, with a voltage between 1800 and 2200 V (to optimize ionization efficiency) applied to the needle, and a counter voltage of 450 V applied to the capillary. Samples were prepared by adding a spray solution of 70:29.9:0.1 (v/v/v) CH_3OH/water/formic acid to a solution of the sample at a v/v ratio of 1 to 5% to give the best signal-to-noise ratio. High-resolution mass spectra were taken on a VG Autospec instrument.

Synthesis and Characterization of the Compounds

2,6-Bis[(*M,M*)-3,5-di(tert-butyl)-8-hydroxy-8-dimethylnona-3,4-diene-1,6-diynyl]pyridine ((*M,M*)-3)

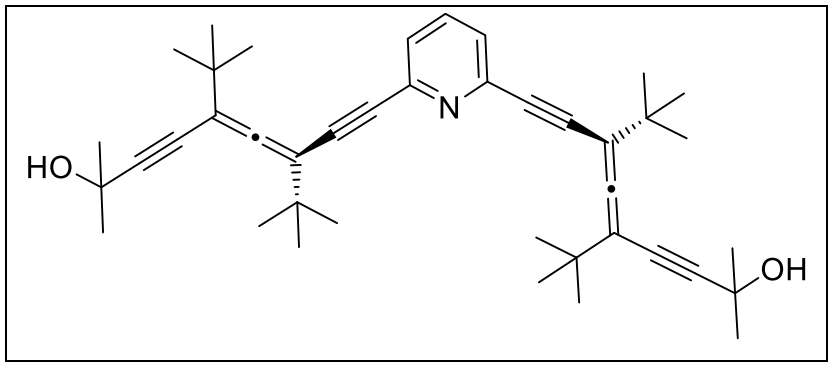

Scheme S1

Two solutions were prepared; *1.* A solution of (*M*)-**2**[2,3] (115 mg, 0.44 mmol) in toluene (5 mL) in a Schlenk tube; *2.* A solution of $[PdCl_2(PPh_3)_2]$ (8 mg, 0.011 mmol) and commercial 2,6-dibromopyridine (48 mg, 0.20 mmol) in toluene (5 mL). Both solutions were degassed with argon. CuI (4 mg, 0.02 mmol) was added to solution 2 and this solution was further degassed with argon. TMEDA (71 mg, 0.61 mmol) was added to solution *1*. Then solution *2* was transferred via cannula to solution *1*. After sparging the reaction mixture, it was stirred at reflux (110 °C) under Ar for 20 h. The reaction mixture was then partitioned between saturated aqueous NH_4Cl solution and hexane. The aqueous phase was extracted with hexane. The combined organic phases were dried (Na_2SO_4) and the solvent was removed under reduced pressure followed by purification by flash chromatography on silica gel (hexane/AcOEt 70:30) afforded (*M,M*)-**3** (95 mg, 79%) as a yellow oil.

$C_{41}H_{53}NO_2$

M.W.: 591.87 g mol^{-1}

^{1}H NMR (400 MHz, $CDCl_3$): δ (ppm) 7.58 (t, *J*= 7.8 Hz, 1H), 7.34 (d, *J*= 7.8 Hz, 2H), 1.55 (s, 12 H, -C(CH_3)$_2$OH), 1.19 (s, 18 H, *t*-Bu), 1.13 (s, 18 H, *t*-Bu).

^{13}C NMR (100 MHz, $CDCl_3$): δ (ppm) 212.1 (C, C=**C**=C), 144.2 (C, py), 136.2 (CH, py), 126.3 (CH, py), 103.5 (C), 102.7 (C), 97.9 (C), 91.5 (C) 84.1 (C), 75.7 (C), 65.8 (C, -C(CH_3)$_2$OH), 35.8 (C, *t*-Bu), 35.6 (C, *t*-Bu), 31.6 (CH_3, -C(**CH_3**)$_2$OH), 29.2 (CH_3, *t*-Bu), 29.0 (CH_3, *t*-Bu).

FT-IR (NaCl) *v* 3361, 2965, 2929, 2901, 2866, 2206, 1557, 1444 cm^{-1}.

UV-Vis ($CHCl_3$): λ_{max} (ε) = 317 nm (20872 L mol^{-1} cm^{-1}), 289 nm (22990 L mol^{-1} cm^{-1}).

HRMS-ESI: *m/z* calc. for $C_{41}H_{54}NO_2^+$ 592.4149; found 592.4156.

$[\alpha]_D^{20}$ = –487 (c= 6.2 x 10^{-4} g/mL, $CHCl_3$)

The enantiomer (*P,P*)-**3** was obtained in a similar manner: **HRMS-ESI***: m/z* calc. for $C_{41}H_{54}NO_2^+$ 592.4149; found 592.4156. **$[\alpha]_D^{20}$** = +463 (c = 5 x 10^{-4} g/mL, $CHCl_3$)

CD and UV/Vis spectra of (*P,P*)-**3** (black solid line) and (*M,M*)-**3** (black dashed line) recorded in $CHCl_3$:

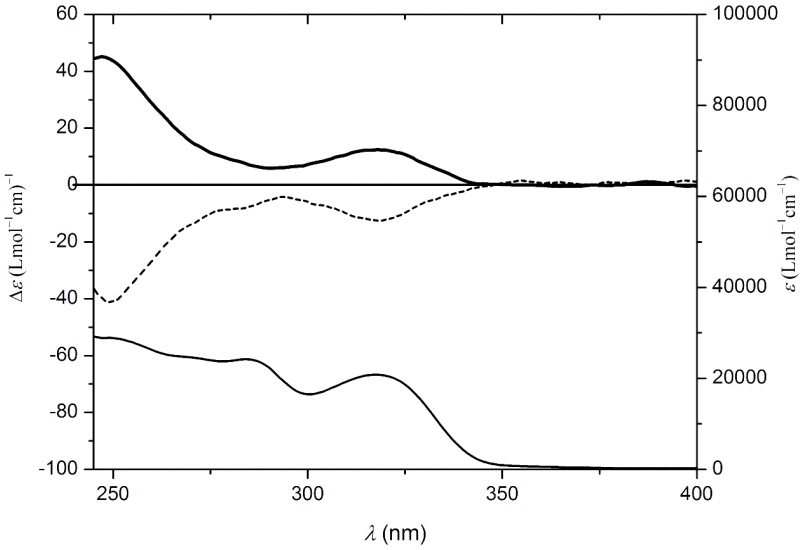

Figure S1

^{1}H-NMR (400 MHz, $CDCl_3$)

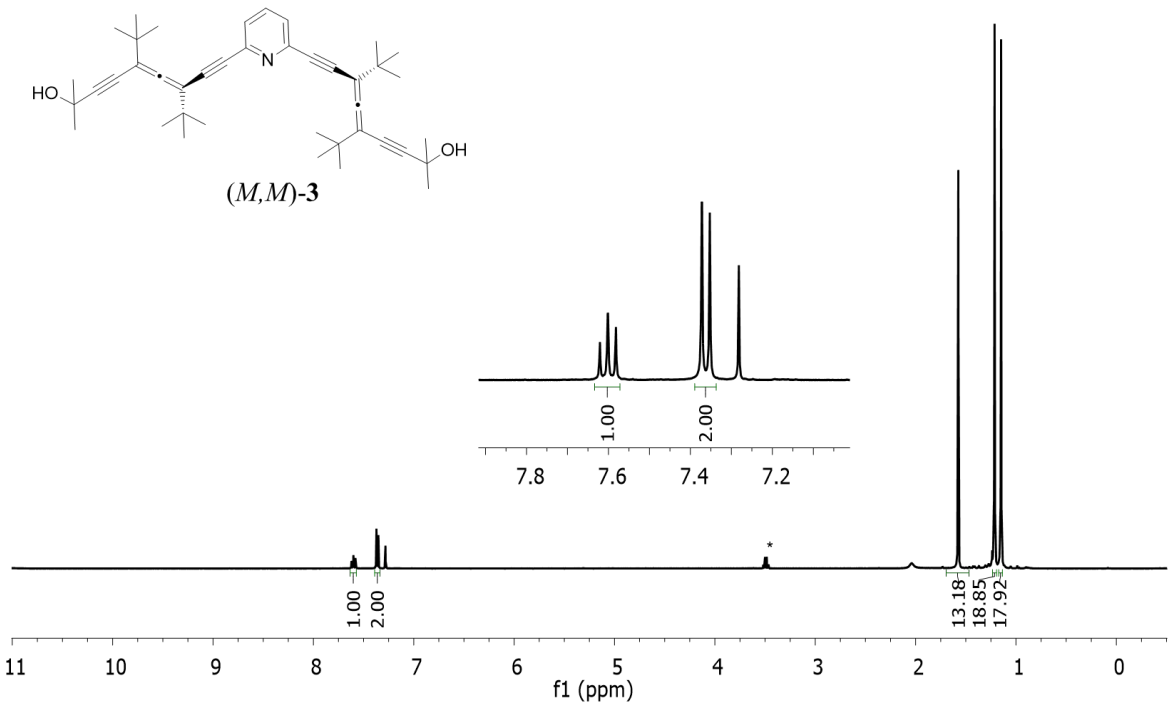

Figure S2

^{13}C-NMR (100 MHz, $CDCl_3$):

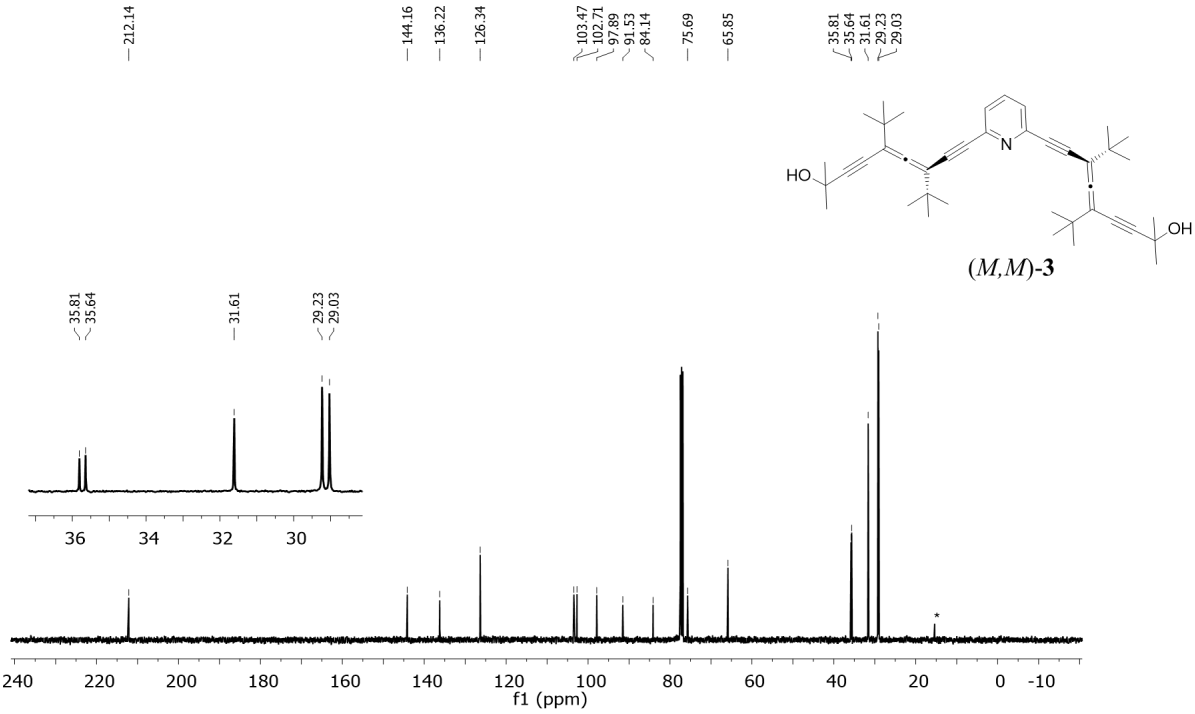

Figure S3

2,6-Bis[(*M*)-3,5-di-*tert*-butylhepta-3,4-dien-1,6-diyn-1-yl)]pyridine ((*M,M*)-1)

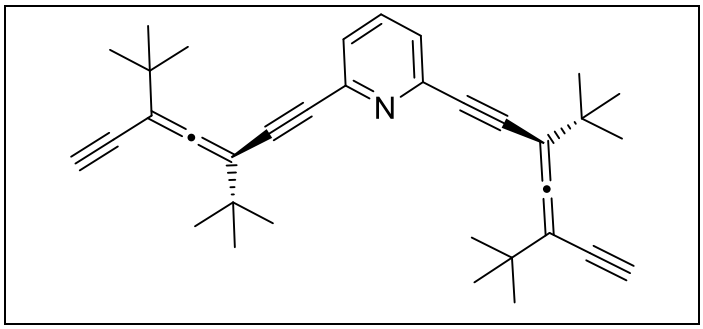

Scheme S2

Pulverized NaOH (732 mg, 18.26 mmol) was placed in a round-bottom flask, and dried with a heat gun under vacuum (10^{-1} Pa) and then, filled with Ar. Enantiopure (*M,M*)-**3** (60 mg, 0.10 mmol) was dissolved in dry toluene (4 mL), and the solution was transferred to the round-bottom flask. The mixture was refluxed at 110 °C for 2 h. Then saturated aqueous NH_4Cl solution was added, and the mixture was extracted with hexane. The combined organic phases were dried with Na_2SO_4. Evaporation *in vacuo* and purification by flash chromatography on silica gel (hexane/AcOEt 8:2) afforded (*M,M*)-**1** (39 mg, 80%) as a white solid.

$C_{35}H_{41}N$

M.W.: 475.32 $gmol^{-1}$

^{1}H NMR (400 MHz, $CDCl_3$): δ (ppm) 7.56 (t, J = 7.8, 1H), 7.32 (d, J = 7.8, 2H), 2.99 (s, 2H, C≡C-H), 1.18 (s, 18H, *t*-Bu), 1.13 (s, 18H, *t*-Bu).

^{13}C NMR (100 MHz, $CDCl_3$): δ (ppm) 212.8 (C=**C**=C), 144.1 (C, py), 136.2 (CH, py), 126.5 (CH, py), 103.2 (C), 103.1 (C), 91.8 (C), 83.7 (C), 81.1 (CH, -C≡C-H), 77.2(C), 35.9 (C, *t*-Bu), 35.5 (C, *t*-Bu), 29.2 (CH_3, *t*-Bu), 29.0 (CH_3, *t*-Bu).

FT-IR (NaCl) ν 3309, 2965, 2930, 2903, 2867, 1571, 1557, 1443, 1239, 1201 cm^{-1}.

UV-Vis ($CHCl_3$): λ (ε)= 317 nm (16917 $Lmol^{-1}cm^{-1}$), 283 nm (18779 $Lmol^{-1}cm^{-1}$)

$[\alpha]_D^{20}$= –289 (c= 4.73 x 10^{-4} g/mL, $CHCl_3$)

HRMS-ESI: *m/z* calc. for $C_{35}H_{42}N^+$ 476.3312; found 476.3317.

HRMS-MALDI: *m/z* calc. for $C_{35}H_{42}N^+$ 476.3312; found 476.3324. *m/z* calc. for supramolecular dimer, $C_{70}H_{83}N^+$ 951.66; found 951.67.

The enantiomer (*P,P*)-**1** was obtained in a similar manner: HRMS-ESI: *m/z* calc. for $C_{35}H_{42}N^+$ 476.3312; found 476.3317. $[\alpha]_D^{20}$ = + 284 (c = 4.75 x 10^{-4} g/mL, $CHCl_3$)

CD and UV/Vis spectra of (*P,P*)-**1** (black solid line) and (*M,M*)-**1** (black dashed line) recorded in $CHCl_3$:

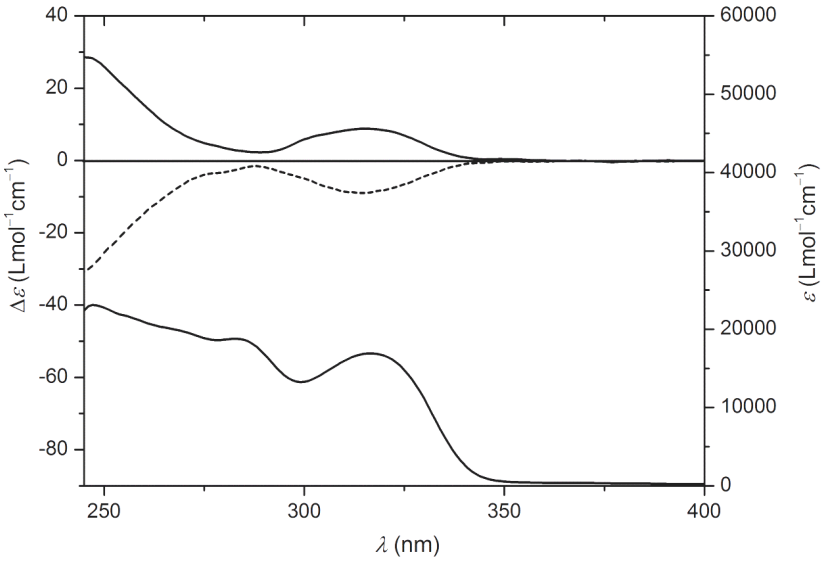

Figure S4

^{1}H-NMR (400 MHz, $CDCl_3$):

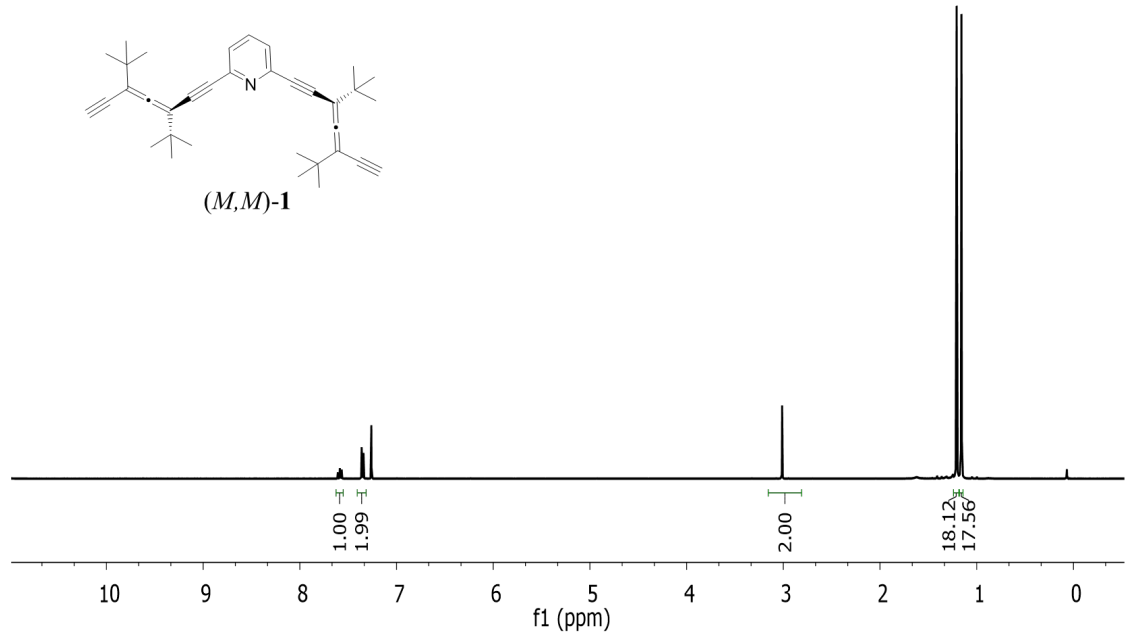

Figure S5

^{13}C-NMR (100 MHz, $CDCl_3$):

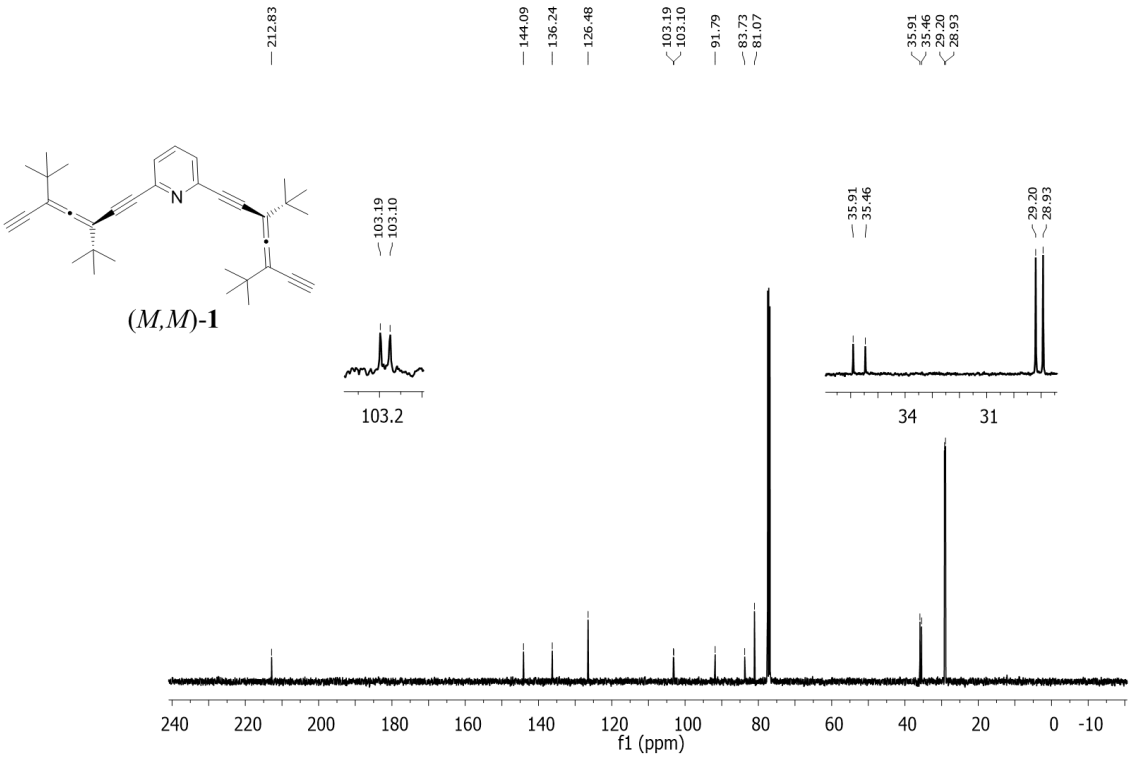

Figure S6

HRMS-ESI experiments at different concentrations of [(*M*,*M*)-1]

Samples were prepared in (acetone)-97% / (water with formic aced 0.1%)-3%

[(*M*,*M*)-**1**] = 2x10^{-4} M ratio monomer/dimer 1/40

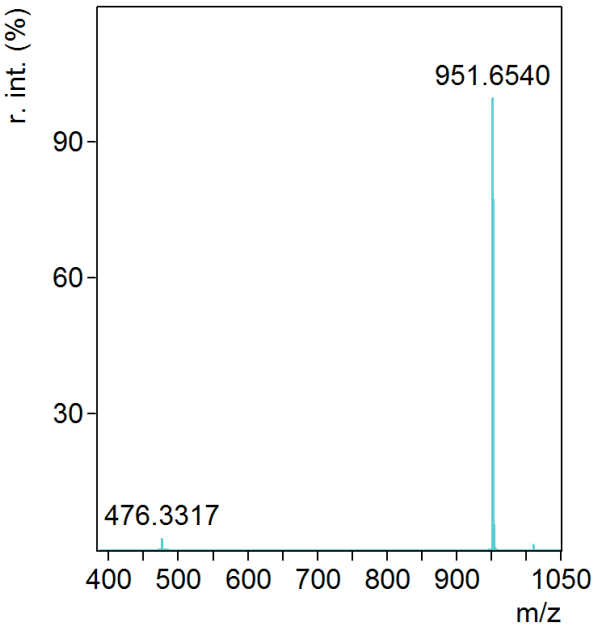

Figure S7

[(*M*,*M*)-**1**] = 2x10^{-5} M ratio monomer/dimer 1/12

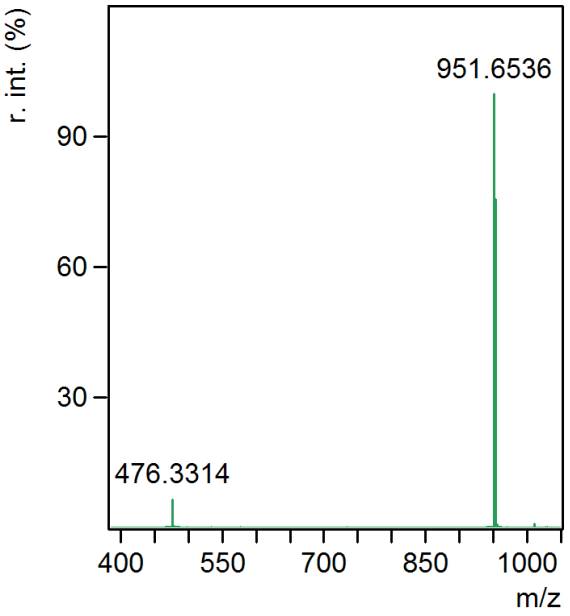

Figure S8

[(*M,M*)-**1**] = 2x10^{-6} M ratio monomer/dimer 1/2

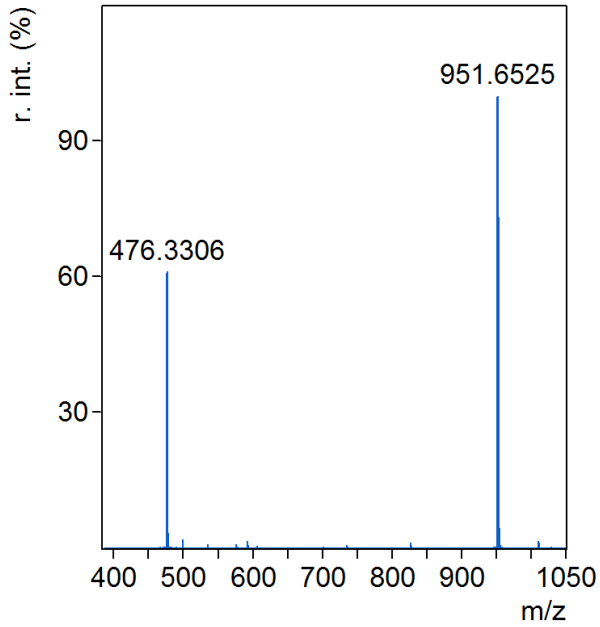

Figure S9

[(*M,M*)-**1**] = 2x10^{-7} M ratio monomer/dimer 10/1

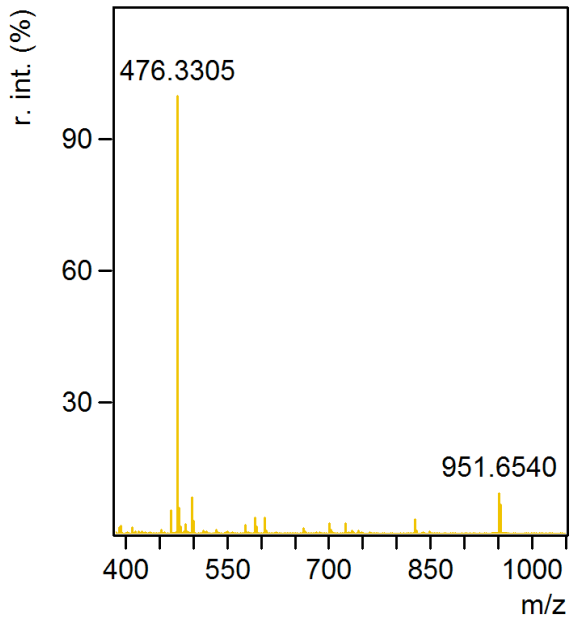

Figure S10

STM studies

The experiments were performed in an ultrahigh vacuum apparatus with a base pressure of less than 2×10^{-10} mbar. The Ag(111) single crystal surface was cleaned by repeated cycles of Ar^+ ion sputtering, followed by annealing to 740 K. The bAPy (*M*,*M*)-**1** were sublimated by organic molecular beam epitaxy (OMBE) from a quartz glass crucible inside a Knudsen cell. The sublimation temperature T_{OMBE} was around 440 K. The temperature of the substrate was kept below 140 K. After the preparation, the sample was cooled down and transferred into our home-made Besocke-type scanning tunnelling microscope (STM), where data were recorded at 5.5 K.

For the quantitative determination of the cell size, we averaged STM images of the same area obtained with four different slow-scan directions to minimize the influence of the thermal drift. The measured parameters of the MM-L unit cell (Fig. 3c) are $a_L = b_L$ = 12.6 ± 0.1 Å and α = 60 ± 2°. The angle θ between the [11−2] direction and $\boldsymbol{a}_L$ of the red unit cell (clockwise) is 66.5 ± 1°. The unit cell referred to as MM-R (Fig. 3c) has the same parameters but with θ' between the [11−2] direction and $\boldsymbol{a}_R$ (counterclockwise) equal to −65.5 ± 1°. The unit cell of *MM*-L domain (red in Fig. 3c) can be written in matrix representation as:

$$\begin{pmatrix} \vec{a_L} \\ \vec{b_L} \end{pmatrix} = \begin{pmatrix} 3 & 2 \\ 5 & -3 \end{pmatrix} \begin{pmatrix} \vec{u} \\ \vec{v} \end{pmatrix}.$$

Similarly, unit cell of *MM*-R domain (red in Fig. 3c) can be written as:

$$\begin{pmatrix} \vec{a_R} \\ \vec{b_R} \end{pmatrix} = \begin{pmatrix} -5 & 2 \\ -2 & -3 \end{pmatrix} \begin{pmatrix} \vec{u} \\ \vec{v} \end{pmatrix}.$$

Possible enantiomeric PP-R and/or PP-L domains were not found, verifying that the chirality of the allene moieties has been preserved.

In-plane orientations of bAPy (*M,M*)-1 dimer on Ag(111)

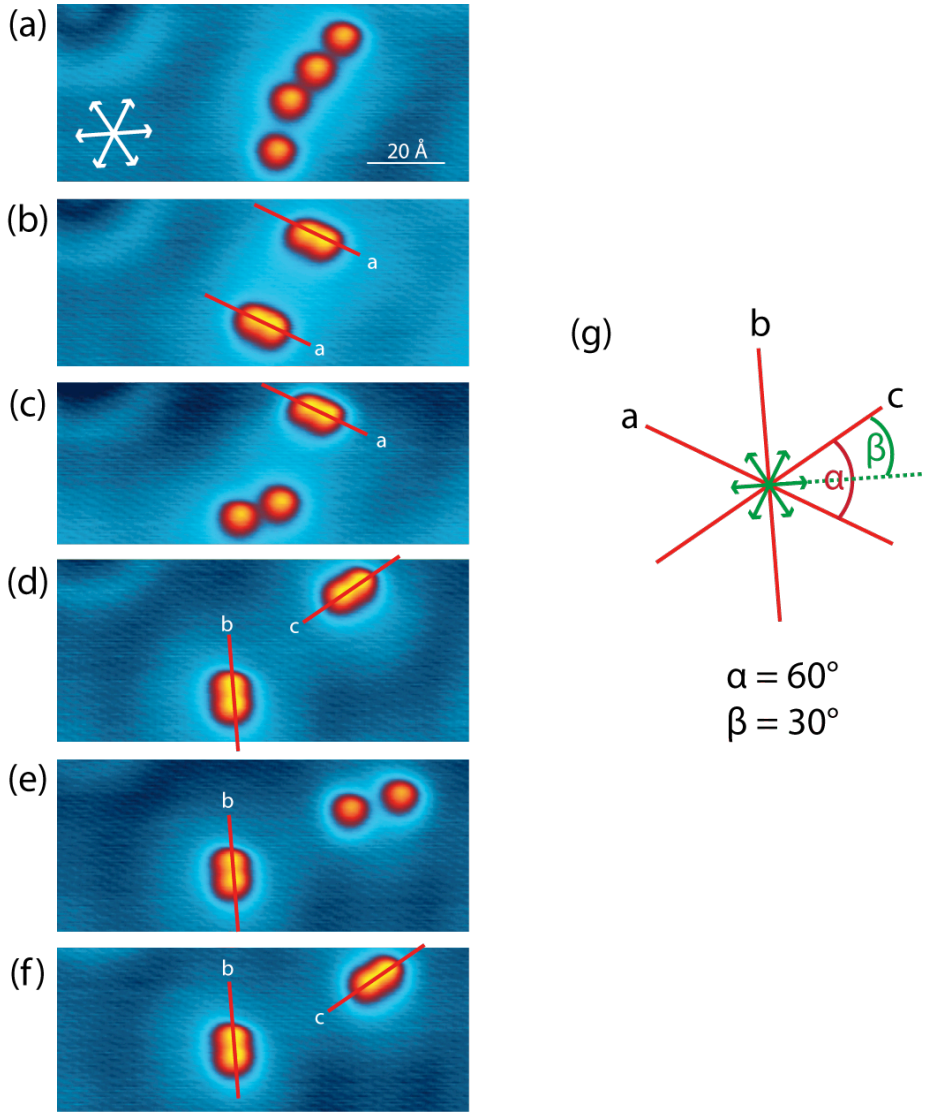

Figure S11. (a)–(f) A sequence of STM tip-manipulation images showing dimer formation and disruption processes. The close-packed directions of Ag(111) are indicated in (a). The red lines in (b)–(f) indicate three prefered orientations of dimer indicated as a, b and c and they are along <–1–12> directions. (g) shows that orientations a, b and c have an angle of 60° with respect to each others. The relative orientation between dimer and substrate close-packed direction is about 30°. Tip manipulation parameters: U_b = 0.6 V, I_t = 0.2 nA.

Translational and rotational movement of bAPy (*M*,*M*)-1 on Ag(111)

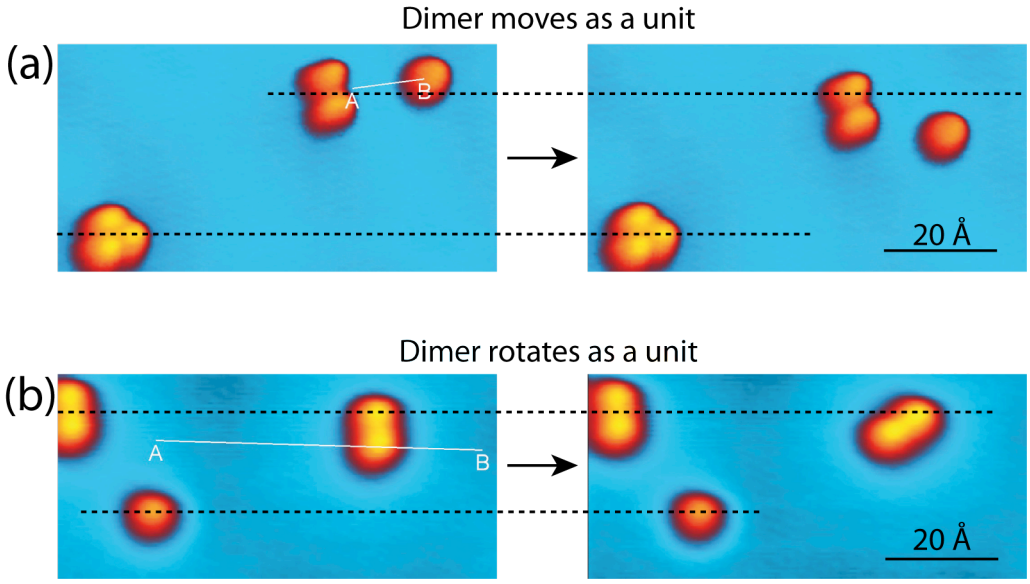

Figure S12. STM images of tip manipulation under constant current mode. (a) dimer moves as a unit. (b) dimer rotates as a unit. A and B denote the starting and ending point of the manipulation. Tip manipulation parameters: U_b = 0.8 V, I_t = 0.2 nA. The black dashed lines are guide to the eyes.

STM images of *MM*-L and *MM*-R domains

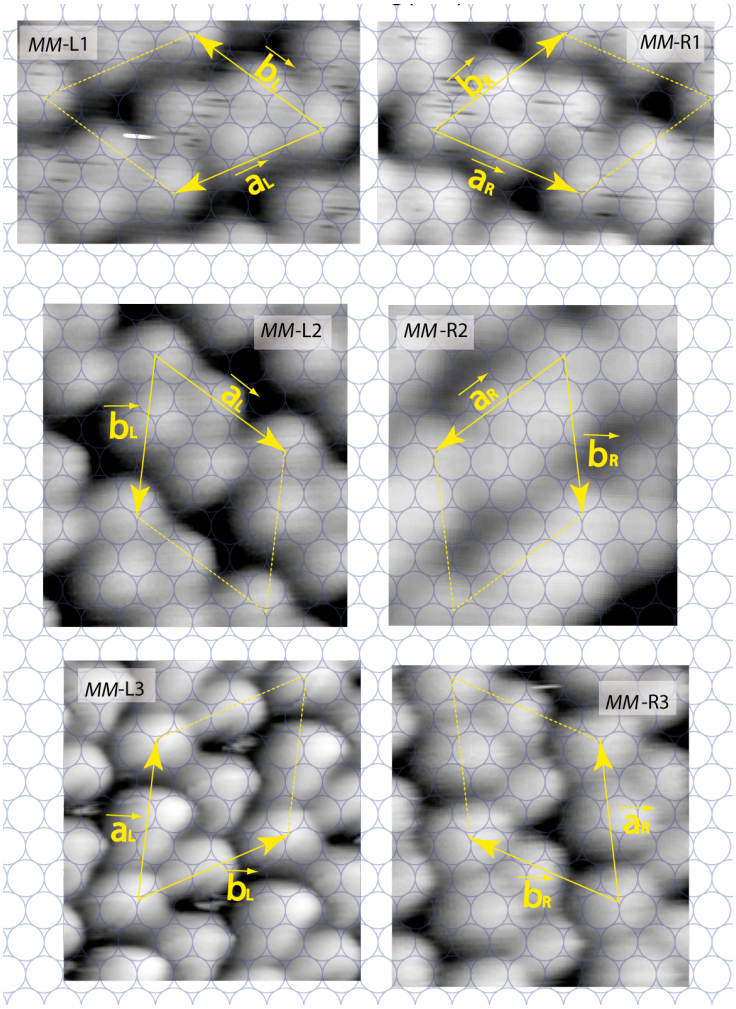

Figure S13. Experimental data of 6 domains. All the images are scaled with the underlying atomic lattice.

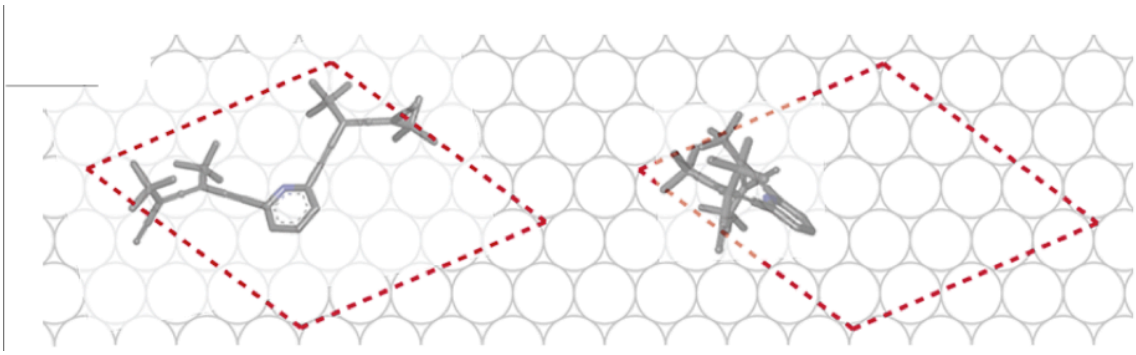

Figure S14. Comparison of experimentally determined unit cell size with approximate (*M,M*)-**1** dimensions in flat (left) and upright (right) orientations.

Diastereomeric features

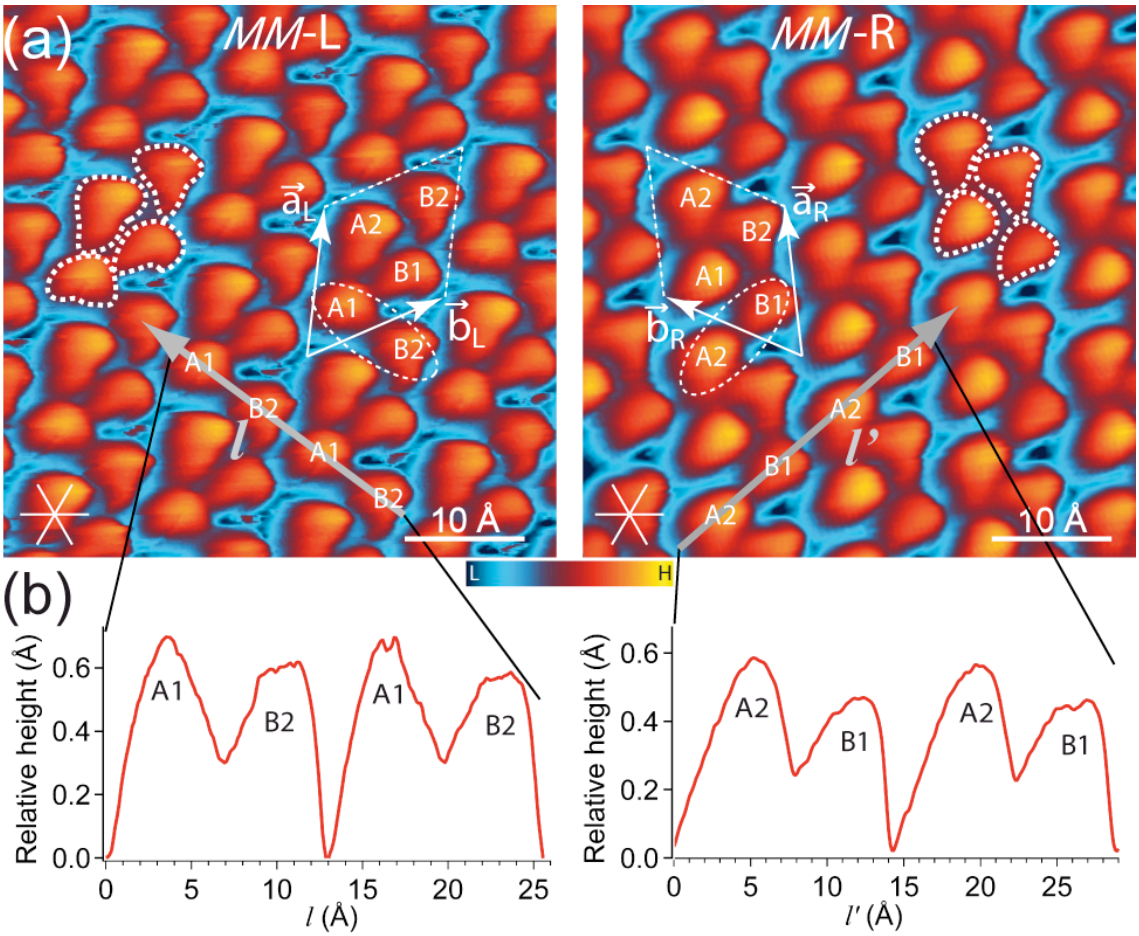

Figure S15. High-resolution STM images of diastereomeric domains: (a) MM-L (U_B = −0.3 V, I_T = 0.1 nA) and MM-R (U_B = −0.35 V, I_T = 0.05 nA). White dashed lines are contours of a single-molecule feature each. (b) Height profiles along mirror-symmetric directions *l* and *l*' marked with gray arrow in (a).

Molecular dynamics simulations

Simulations were performed with the program C36b2 CHARMM[4] using the MMFF package implementation[5] with infinite substrate slab when indicated and infinite cutoffs. The Langevin thermostat was employed with a friction coefficient of 1 ps^{-1}. A time step of 2 fs was employed using the SHAKE implementation[6] for the Hydrogen atoms. The chiral allene-dihedrals (for the (*M,M*)-**1** enantiomer) were doubly constrained using a harmonic constant of 15 kcal/mol.

In order to elucidate the structure for the formation of the dimers, constant temperature simulations at 200 K were performed at conditions representative of the ESI experiments, i.e. in gas phase for one molecule alone (infinite dilution) and for 100 molecules in a 1000 Å box (~0.1 mM) (Figure S16). The dihedral analysis for the dilute system (Figure S16a) shows that the molecule in the "closed-closed" dihedral conformation **C** is preferred. Conversely, the "closed-open" conformation "**B**"" is preferred when one molecule is analysed at the 0.1 mM concentration conditions in Figure S16b. The latter conformation, undergoes supramolecular self-recognition to its partner "open-closed" molecule, via a high van der Waals (vdW) contact surface as illustrated in Figure S17. These studies show that shape-specific conformations (i.e. dihedral angles ϕ_1 and ϕ_2 between the pyridine cores and the ADTE units) are playing a role in gas phase molecular recognition. Thus, a general definition for shape-specific molecular recognition is put forward to address this phenomenon: Morphological self-assembly is defined as the optimization of a molecule's morphology to allow highly specific shape-complementary molecular recognition (see Figure S17) even though the driving van der Waals force is by itself non-directional and unspecific.

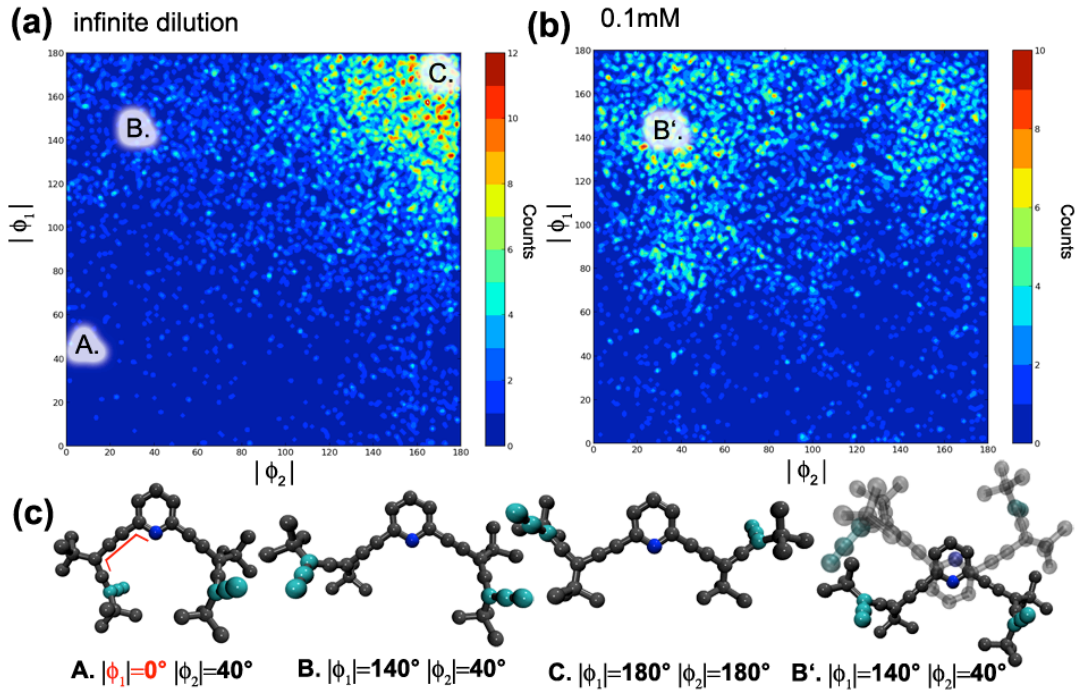

Figure S16 (a) The single-molecule gas phase absolute dihedral conformational map of (*M,M*)-**1** obtained by ns-long MD calculations at 200 K showing the occupation probability of the different conformations and where the conformers **A**-**C** are located. (b) The gas phase dihedral conformation map using 100 molecules in a 0.001 μm^3 volume. The most populated dimer conformer **B'** is shown in (c). Its partner molecule is also shown on top with transparent atoms. Hydrogens are not shown and the acetylene moieties are shown in cyan. (c) Common conformers. **A** open-open, **B** open-closed, **C** closed-closed and **B'**, a open-closed, closed-open dimer.

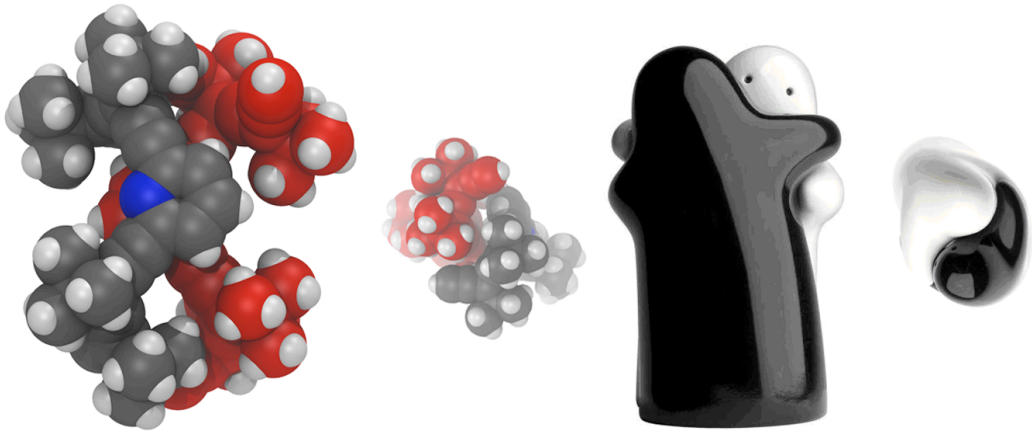

Figure S17. Morphological self-assembly of a closed-open, open-closed dimer as present in conformation **B'**. The high vdW contact chiral supramolecule is reminiscent of the salt&pepper design on the right.

Motivated by the large dihedral conformational space for morphological self-assembly of (*M,M*)-**1,** we set to unravel the most stable STM conformer structure by means of molecular dynamics quenching. For this, ns-long MD simulations were performed for all different morphologically assembled dimers as starting structures (Figure S18). The simulations started at 250 K and were quenched to 50 K as shown in Figure S19.

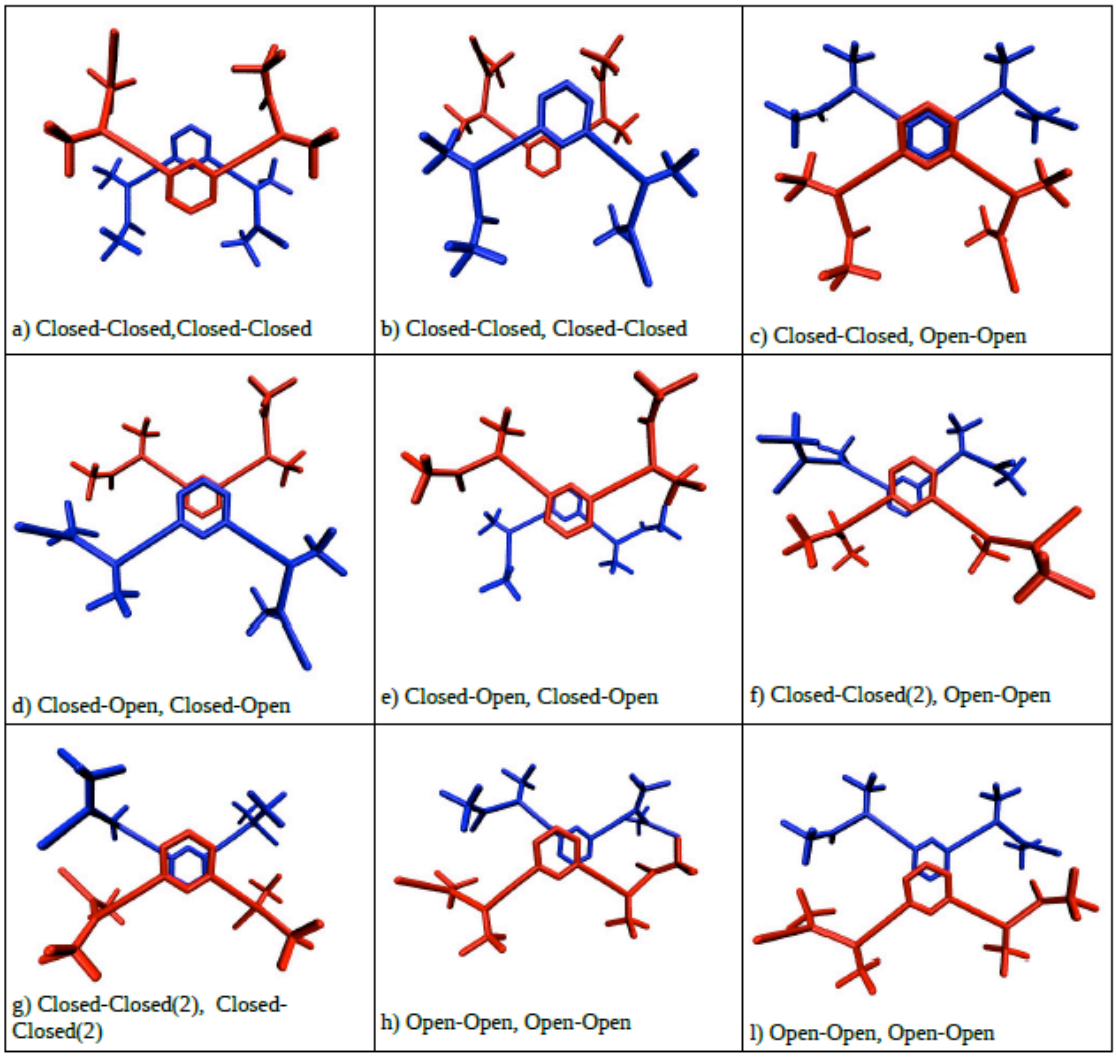

Figure S18. Starting configuration guesses for gas phase temperature-quenching molecular dynamics of a (*M,M*)-**1** dimer. All the initial guesses exhibit antiparallel pyridine configuration since the parallel (same side Nitrogen) pyridines were overall energetically unfavored. As in Figure S16, the notation "closed" or "open" qualitatively referes to the freely rotating dihedral angle of the pyrine with respect to the allenes.

1. Closed-Closed, Open-Open Dimer

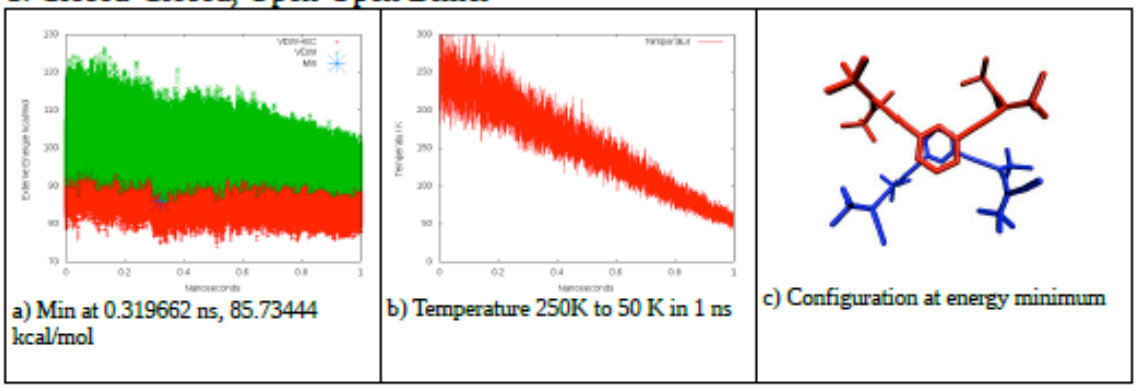

a) Min at 0.319662 ns, 85.73444 kcal/mol

b) Temperature 250K to 50 K in 1 ns

c) Configuration at energy minimum

2. Open-Open, Open-Open Dimer

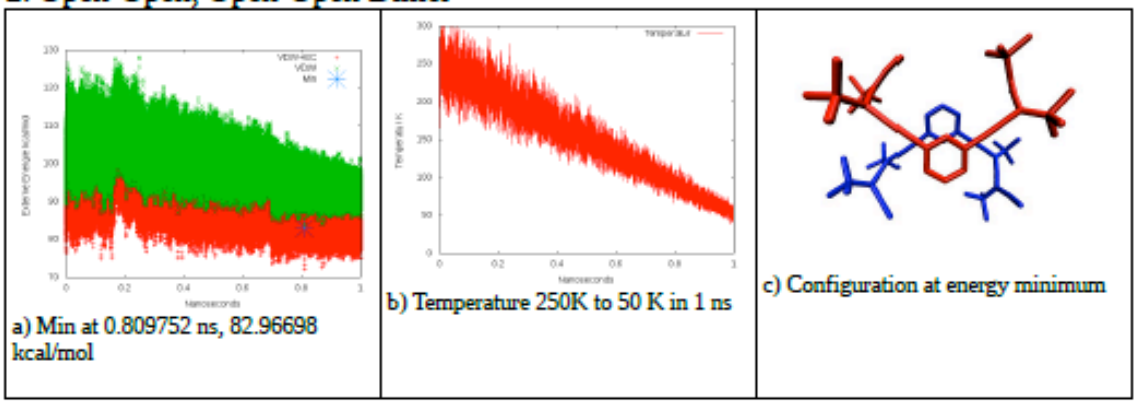

a) Min at 0.809752 ns, 82.96698 kcal/mol

b) Temperature 250K to 50 K in 1 ns

c) Configuration at energy minimum

3. Closed-Closed, Closed-Closed Dimer

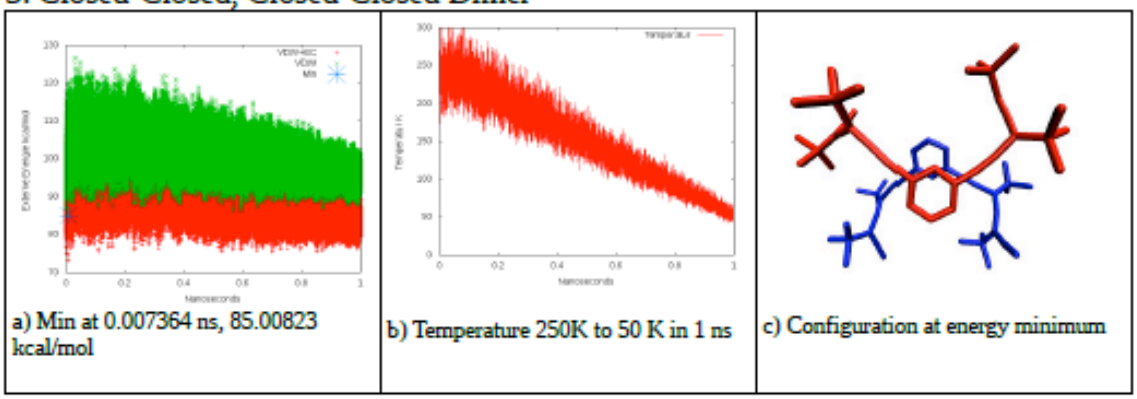

a) Min at 0.007364 ns, 85.00823 kcal/mol

b) Temperature 250K to 50 K in 1 ns

c) Configuration at energy minimum

Figure S19. Lowest vdW energy structures extracted from cooling experiments ($T_{initial}$ = 250 K, T_{final} = 50 K) showing partial "hugging". The simulations were conducted up to three times independently, for each initial guess in Figure S18. Notice how all the final dimers from three different initial conformations feature antiparallel overlap between the terminal allene-ditertbutyl-ethylene units, closely resembling the open-closed, open-closed dimer "hugs", initially found in the gas-phase search in Figure S16 and shown also in Figure S17. (As a guide to the eye, note how the dihedrals on the right hand side of the molecules are all "closed", i.e. in an dihedral angle close to 180°.). The green plot in the l.h.s. figures is the external energy wihout electrostatic interactions, i.e. only the MMFF C7-C14 vdW potential for carbon type 5 and hydrogen 2. The red l.h.s. plot includes also external inter- and intra- molecular electrostatics.

Finally, two dimers as-elucidaded in Figure S19 were combined to afford Fig. 4a in the main text after simulation at 20 K for 1 ns and explicit parameterization of a Ag(111)-mimic substrate. This substrate consists on three slabs of silver merged together in a single plane, whereby the Ag(111) top-site has a charge of -0.4 and the rest reach charge neutrality.[7] Every silver atom uses the type 3 atom MMFF C7-C14 vdW potential. Note that at these temperatures and simulation times scales, the simulations of the tetramer structure alone on Ag(111) do not recover a "hug" (i.e. antiparallel overlap between the terminal allene-ditertbutyl-ethylene units, see Fig. 4a, black/white arrows). This tetramer was further simulated at 200 K using periodic boundary conditions, i.e. a monolayer with corresponding unit cell of a = 15 Å , **b** = 15 Å and **(a,b)**=60° for 10 ns. A slightly larger unit cell and temperature (in contrast with the experiments, see main text) was employed in order to observe rotations along the dihedral which would increase the surface contact therby minimizing the vdW energy an recovering a "hug" motif. In fact, already after 2 ns a step transition to a "hug" was observed (Fig. S20, Fig 4b-d, arrows).

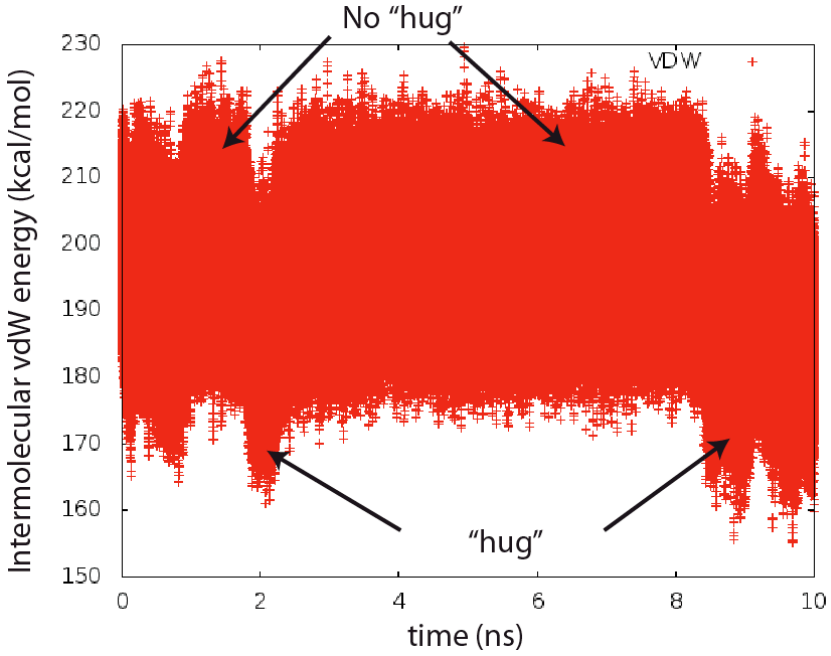

Figure S20. vdW energy for the monolayer shown in Fig. 4b-d, main text.

The "Surface" implementation in CHARMM with rprobe 0 and vdW radius for all atoms of 2.6 Å was used to obtain the accessible surface areas (ASA) of interest. The intersection of the ASA of interest with the total ASA in the vdW complex was then computed and used accordingly to obtain the vdW molecular surface contact area (MSCA see provided scripts in the online material).

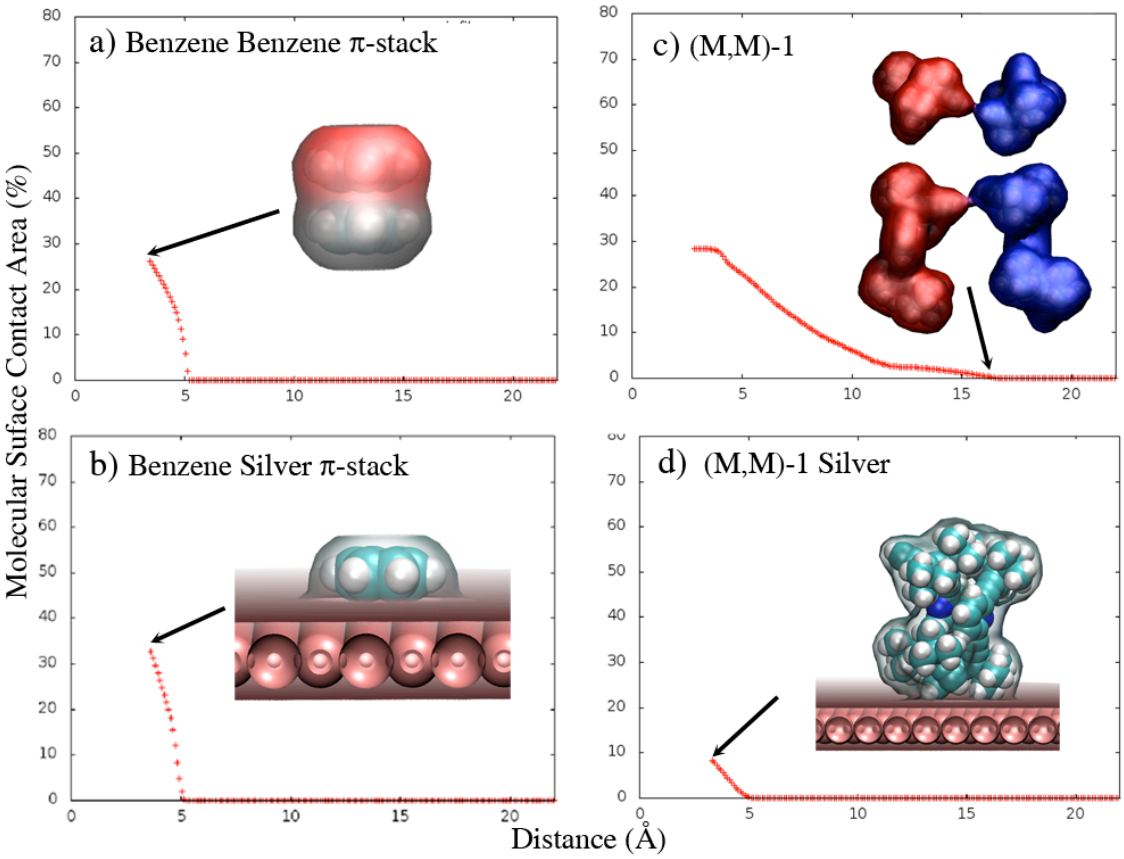

Figure S21. VdW molecular surface contact area (MSCA) as a percentage of the total area of molecule of interest. a,b) Prototypical cases in the benzene dimer complex (MSCA 27 %) and benzene adsorption on silver (MSCA 33 %). **c,d)** MSCAs for the dimer of Fig. 1 main text. The MSCA of one monomer in the dimer is 29% and of a whole dimer with the silver is 9%. The translucent surfaces in the insets' images are set close to the calculated ones.

Code and Scripts

Scripts and structures used are made available in the Online Supporting Material in accordance to the guidelines of Responsible Conduct in Computational Research www.rcecer.org.

References

(1) Perrin, D.; Armarego, W. *Purification of Laboratory Chemicals*; Pergamon Press: Oxford, 1998.

(2) Alonso-Gómez, J. L.; Rivera-Fuentes, P.; Harada, N.; Berova, N.; Diederich, F. *Angew. Chem. Int. Ed.* **2009**, *48*, 5545.

(3) Alonso-Gómez, J. L.; Rivera-Fuentes, P.; Harada, N.; Berova, N.; Diederich, F. *Angew. Chemie* **2009**, *121*, 5653.

(4) Brooks, B. R.; Brooks, C. L.; Mackerell, A. D.; Nilsson, L.; Petrella, R. J.; Roux, B.; Won, Y.; Archontis, G.; Bartels, C.; Boresch, S.; Caflisch, A.; Caves, L.; Cui, Q.; Dinner, A. R.; Feig, M.; Fischer, S.; Gao, J.; Hodoscek, M.; Im, W.; Kuczera, K.; Lazaridis, T.; Ma, J.; Ovchinnikov, V.; Paci, E.; Pastor, R. W.; Post, C. B.; Pu, J. Z.; Schaefer, M.; Tidor, B.; Venable, R. M.; Woodcock, H. L.; Wu, X.; Yang, W.; York, D. M.; Karplus, M. *J. Comput. Chem.* **2009**, *30*, 1545.

(5) Halgren, T. A. *J. Comput. Chem.* **1996**, *17*, 490.

(6) Ryckaert, J. P.; Ciccotti, G.; Berendsen, H. J. C. *J. Comput. Phys.* **1977**, *341*, 327.

(7) C. A. Palma, J. Björk, F. Rao, D. Kühne, F. Klappenberger, and J. V. Barth, Nano Lett. in press, (2014), DOI 10.1021/nl5014162.